This is the accepted manuscript made available via CHORUS. The article has been published as:

Orientations of low-energy domain walls in perovskites with oxygen octahedral tilts

Fei Xue, Yijia Gu, Linyun Liang, Yi Wang, and Long-Qing Chen

Phys. Rev. B **90**, 220101 — Published 1 December 2014

DOI: 10.1103/PhysRevB.90.220101

Orientations of Low-Energy Domain Walls in Perovskites with Oxygen Octahedral Tilts

Fei Xue, Yijia Gu, Linyun Liang, Yi Wang, and Long-Qing Chen

Department of Materials Science and Engineering, The Pennsylvania State University, University Park, Pennsylvania 16802, USA

Abstract:

Many applications of ferroic materials, such as data storage and spintronics, are achieved through the control and manipulation of their domain wall (DW) orientations and configurations. Here we propose a new condition, the rotational compatibility condition, to identify low-energy DWs in perovskites with oxygen octahedral tilt instability. It is derived from the strong DW energy anisotropy arising from the rigidity and corner-sharing feature of the octahedral network. We analyze quantitatively the DWs in $SrTiO_3$ and explain successfully the unusual ferroelectric DW width and energy in $BiFeO_3$.

PACS numbers: 77.84.-s, 68.35.-p, 77.80.Dj, 81.30.-t

Perovskites (ABO_3) are one of the most studied families of functional materials that may exhibit a variety of interesting properties including ferroelectric (FE), magnetic, catalytic, ion conducting, and superconducting with applications to energy storage and conversion devices.[1, 2] The functional versatility of perovskites is partially due to their adaptable structure which can accommodate more than half of the elements from the periodic table in A or B sites.[1] A typical characteristic of the perovskite structure is the corner-sharing network of the rigid BO_6 oxygen octahedra which can rotate or tilt as a whole with almost no distortion of the O-B bonds.[2] More importantly, it is found that the oxygen octahedral tilts (OTs) are strongly coupled to the microscopic electronic, magnetic, and optical properties.[3-5] Domain walls (DWs) as the

symmetry breaking elements of OTs are thus expected to give rise to new physical properties through coupling between OTs and other order parameters, which in turn may alter the overall macroscopic responses of a material. It is suggested that these functional DWs may potentially be used as new elements for nanoelectronics.[6]

The orientations of permissible (low-energy) DWs are conventionally determined using two conditions: one is the mechanical compatibility condition which requires matching of the atomic displacements of the two adjacent domains to minimize the strain energy;[7] the other is the electrical neutrality condition to minimize the electrostatic energy, e.g. in FE DWs arising from the bound charges. These two conditions are, however, insufficient to predict the orientations of the low-energy OT DWs. To overcome this difficulty, here we propose a third condition, "rotational compatibility condition".

We first derive the rotational compatibility condition from the specific corner-connecting configuration of the oxygen octahedra in perovskites, inferring a universal and strong anisotropy in the OT DW energy. We apply the condition to ferroelastic $SrTiO_3$ (STO), and the anisotropic DW energies are calculated based on the Ginzburg-Landau-Devonshire (GLD) theory. We then investigate the interaction between the OTs and the FE polarization in multiferroic $BiFeO_3$ (BFO) and show that the anisotropy of the OT DW energies may drastically alter the relative stability of different types of FE DWs.

Let us start from the oxygen octahedral network of the perovskite structure and choose the Cartesian coordinate system along the crystallographic directions of the pseudocubic lattice. Due to the corner-sharing feature and rigidity of the oxygen octahedra, the rotation of one octahedron along the x_3 direction requires the rest of octahedra within the same layer (x_1-x_2 plane)

to rotate accordingly, as shown in Fig. 1 (a) and (b). Thus, all the corner-connected octahedra rotate in opposite directions in an alternate pattern leading to a unit-cell doubling. On the other hand, the oxygen octahedra in the adjacent layers are free to rotate in either the same or opposite pattern, which gives rise to the so-called in-phase tilt (Fig. 1b) or out-of-phase tilt (Fig. 1a), respectively. In an out-of-phase tilt, the unit cell is doubled along all the three pseudocubic axes.[8] Since all the OTs can be decomposed into tilt components along the three pseudocubic axes due to the rigidity of the oxygen octahedra, a general OT pattern can thus be expressed using the Glazer notation.[8] In the following we will discuss the rotational compatibility condition using STO as an example.

The crystal structure of the tetragonal STO, Glazer notation $a^0a^0c^-$, has only one out-of-phase OT component along the x_3 direction. The antiphase DWs in STO would normally be considered to be isotropic since both the mechanical compatibility and electrical neutrality conditions are not applicable. To demonstrate the effect of the rotational compatibility condition on DWs, we focus our discussion on two distinct types of antiphase DWs. The type-I DWs, as shown in Fig. 1 (e), are perpendicular to x_3. Both the neighboring domains produce a zero displacement of the shared oxygen atoms, resulting in almost no disruption in the oxygen positions. Therefore, they are very thin, and the two oxygen octahedral layers across the DWs show the in-phase tilt pattern. This type of DWs are also called "easy walls" with a small DW width and energy.[9] These DWs are analogies to the translational DWs,[10] related to the unit-cell doubling induced by the OTs. The type-II DWs are sketched in Fig. 1 (g). They are parallel to x_3, and the neighboring domains tend to displace the shared oxygen atoms at the DWs in opposite directions. To connect the two domains, the OTs near the DWs have to rotate relative to the two domains, i.e. the oxygen octahedra tilt around x_1 or x_2 axis near the DW. As a result, the DWs

have a much wider thickness with a significantly higher energy comparing to the type-I DWs. With the assumption that the rotations of OTs near a DW cost energy, we propose the rotational compatibility condition to determine the orientations of the low-energy OT DWs in perovskites [proof see supplementary materials]:

$$(\theta_i - \theta_i')n_j = 0(j \neq i), \text{ with } \theta_i = -\theta_i' \neq 0, \quad (1)$$

where θ_i *and* θ_i' *are axial vectors and denote the OT components in the two neighboring domains, and* $\boldsymbol{n}$ *is the DW normal.*

If the OTs only change the sign of *i*th component, i.e. $\theta_j = \theta_j'(j \neq i), \theta_j = -\theta_j' \neq 0(j = i)$, from Eq. (1), we obtain $n_j = 0(j \neq i)$ and the value of n_i is arbitrary, i.e. the wall normal is along the x_i axis. The DW is rotationally compatible with respect to all the changed components, and we call it a fully rotation-compatible DW, usually accompanied by the lowest DW energy in a system. Also, an antiphase DW with the sign changes of two or three OT components, i.e. $\theta_i = -\theta_i' \neq 0, \theta_j = -\theta_j' \neq 0,$ with $j \neq i$, with the wall normal along the x_i axis, is rotationally compatible with respect to the θ_i component, but rotationally incompatible to other flipped components. We call it a partially rotation-compatible DW, with a higher energy than a fully rotation-compatible DW. The rotational compatibility condition does not apply to an OT component that changes to zero, i.e. $\theta_i \neq 0, \theta_i' = 0$.

R. Beanland developed a mathematical framework to describe the effect of the corner-connectivity and symmetry operations, and proposed a method to predict all the symmetry-allowed DW structures.[11] Here Eq. (1) determines that among those allowed by symmetry, the DWs maintaining corner-connectivity with reduced rotations of OTs near the DWs have lower-

energy. More detailed discussions about how Eq. (1) is related to Beanland's description as well as the mechanical compatibility condition are given in supplementary materials.

By applying the rotational compatibility condition, we can readily predict the orientations of the low-energy OT DWs. Examples of several popular perovskite structures with fully rotation-compatible DWs are listed in Table I. Relative to the Glazer notation for the two domains, there is a sign change for only one superscript for the local structure of a DW, either from + to –, or vice versa. In other words, one OT component changes from in-phase to out-of-phase at the DW, or vice versa. For example, at the low-energy DW of an $a^0b^-b^-$ structure, shown in Fig. 1(h), the OTs of the two adjacent domains produce the same displacements for the shared oxygen atoms at the DW, and the local DW structure is $a^0b^-c^+$.

The anisotropy of the OT DWs in STO can be quantitatively analyzed within the GLD framework. For simplicity, the stress-free boundary condition is assumed, and the elastic energy contribution is neglected. The total free energy of the OT domains can then be written as the function of the OT order parameters,

$$F_{OT} = \int (\beta_{ij}\theta_i\theta_j + \beta_{ijkl}\theta_i\theta_j\theta_k\theta_l + \frac{1}{2}\kappa_{ijkl}\theta_{i,j}\theta_{k,l})dV, \quad (2)$$

where V is the system volume; β_{ij} and β_{ijkl} are Landau coefficients; κ_{ijkl} are gradient energy coefficients, and a comma in the subscript stands for spatial differentiation. Assuming that the only active OT is along x_3, type-I DWs (wall normal along x_3) should have a much smaller DW energy than that of type-II DWs (wall normal along x_2), implying $\kappa_{3333} = \kappa_{11} << \kappa_{3232} = \kappa_{44}$. From experimental phonon dispersion data,[9, 12, 13] $\kappa_{11} = 0.28 \times 10^{10}$ J/m^3 and $\kappa_{44} = 7.11 \times 10^{10}$ J/m^3, which agrees quite well with our prediction.

To predict the DW energy anisotropy with an arbitrary orientation for the antiphase DWs in STO, we calculate the energies and widths of the DW with the normal $(1,\omega,\eta)$ in a spherical coordinate system, where η is the polar angle between the normal and x_3. Assuming that no OT components along the x_1 and x_2 axes develop at the DW, we obtain the DW width $\delta = 2\sqrt{-\frac{\kappa_{eff}}{\beta_1}}$, and DW energy $\gamma = \frac{2}{3\beta_{11}}\sqrt{-\beta_1^3 \kappa_{eff}}$, where the effective gradient energy coefficient $\kappa_{eff} = \kappa'_{2323}\sin^2\eta + \kappa'_{3333}\cos^2\eta$ in which κ'_{ijkl} is the gradient energy coefficient tensor in a rotated coordinate system [see supplementary materials]. The DW energy anisotropy depends only on κ_{eff}, whose magnitude along the direction (ω,η) is plotted as a function of the radial distance in Fig. 2(a). The nearly isotropic DW energy in the x_1x_2 plane is due to the relation $\kappa_{12} \sim -\kappa_{44}$.[9] The maximum value corresponds to the DWs that have their normal lying within the x_1x_2 plane. They correspond to the high-energy DWs, and a particular example is the type-II DWs discussed previously. In order to better visualize the κ_{eff} surface, a cross section along the x_1x_3 plane is plotted in Fig. 2(b). The minimum of κ_{eff} is realized when the wall normal is along the x_3 axis, as expected. The calculated anisotropy in κ_{eff} corresponds to the DW energy anisotropy, consistent with the predictions from the rotational compatibility condition. Therefore, the rotational compatibility condition originated from the atomistic characteristics of the OTs can be well modeled by the continuum GLD theory by considering the strong anisotropy of the gradient energy coefficients.

The OTs are usually not the sole order parameters that exist in perovskites, and they typically interact with other order parameters such as polarization, strain and so on. To

understand the influence of the OTs on the FE DW energy anisotropy, we consider BFO as an example.

To describe the OT and polarization DWs in BFO, we adopt the notation $[P_iP_jP_k,\theta_i\theta_j\theta_k](n_in_jn_k)[P_i'P_j'P_k',\theta_i'\theta_j'\theta_k']$, where $[P_iP_jP_k,\theta_i\theta_j\theta_k]$ and $[P_i'P_j'P_k',\theta_i'\theta_j'\theta_k']$ are the polarization and OT components in two adjacent domains. In a given rhombohedral BFO domain, the polarization and out-of-phase OTs are along one of the eight body diagonal <111> pseudocubic directions.[14] For a particular polarization direction, there are two possible OTs, either parallel or antiparallel to the polarization. The two cases are illustrated with one dimensional (1D) schematic drawings of a FE+OT DW and a pure FE DW in Fig. 3(a) and (b), respectively. Therefore, the total number of domain variants is 16 rather than 8. With *u* and *v* labeling the numbers of how many components the polarization and OTs change sign across a DW, their relationship can be either $u+v=3$ for an OT phase shift across the DW, or $u=v$ for no phase shift.[15] Therefore, the possible pairs for values $\{u,v\}$ are $\{0,3\}$, $\{1,1\}$, $\{1,2\}$, $\{2,1\}$, $\{2,2\}$, $\{3,0\}$, and $\{3,3\}$. $\{0,3\}$ corresponds the antiphase OT DWs, and here we only analyze the DWs with low Miller indices. For example, in $[111,111](n_in_jn_k)[111,\bar{1}\bar{1}\bar{1}]$, $(n_in_jn_k)$ is $(100),(110)$ or $(1\bar{1}0)$. (100) is partially rotation-compatible and should have the lowest DW energy among the three. To satisfy the mechanical compatibility and electrical neutrality conditions, the DW orientations of $\{1,1\}$, $\{1,2\}$, $\{2,1\}$, and $\{2,2\}$ can be uniquely determined, and $\{3,0\}$ and $\{3,3\}$ DWs each have one low Miller index DW.[16] Therefore, based on the two conventional conditions, we have a total of nine possible types of DWs as listed in Table II. Only the $[\bar{1}11,\bar{1}11](100)[\bar{1}\bar{1}\bar{1},111]$ DW is fully rotation-compatible, and thus its DW energy should be the lowest among the nine.

To further investigate the consequence of order parameter coupling between the OTs and polarization on the DW energy anisotropy and the order parameter profiles across the DWs in BFO, we employ the GLD theory and phase-field method. We consider all the important energy contributions: bulk chemical energy, gradient energy, elastic energy and electrostatic energy,[17, 18] i.e.

$$F = \int_V [\alpha_{ij} P_i P_j + \alpha_{ijkl} P_i P_j P_k P_l + \beta_{ij} \theta_i \theta_j + \beta_{ijkl} \theta_i \theta_j \theta_k \theta_l + t_{ijkl} P_i P_j \theta_k \theta_l + \frac{1}{2} g_{ijkl} P_{i,j} P_{k,l} + \frac{1}{2} \kappa_{ijkl} \theta_{i,j} \theta_{k,l} + \frac{1}{2} c_{ijkl} (\varepsilon_{ij} - \varepsilon_{ij}^0)(\varepsilon_{kl} - \varepsilon_{kl}^0) - \frac{1}{2} E_i P_i \,] dV \quad (3)$$

where α_{ij}, α_{ijkl} are the Landau coefficients of polarization; t_{ijkl} are coupling coefficients between the polarization and OTs; g_{ijkl} are gradient energy coefficients of polarization; c_{ijkl} is the elastic stiffness tensor; ε_{ij} and ε_{kl}^0 are the total strain and eigen strain, respectively; electric field $E_i = -\varphi_{,i}$ with φ the electrostatic potential. The eigen strain is related to the polarization and OTs through $\varepsilon_{ij}^0 = \lambda_{ijkl} \theta_k \theta_l + h_{ijkl} P_k P_l$, where λ_{ijkl} and h_{ijkl} are coupling coefficients. All the coefficients can be found in supplementary materials. It should be noted that the relation $\kappa_{11} << \kappa_{44}$ is satisfied in describing the energy anisotropy of the OT DWs.

The order parameter profiles across the DWs between different pairs of domains and the corresponding DW energies are obtained by numerically solving the phase-field equations.[19] Periodic boundary conditions are imposed along all three dimensions. The system size is $4096\Delta x \times 1\Delta x \times 1\Delta x$ and the grid spacing is $\Delta x = 0.031 nm$. The coordinate system is rotated if necessary to guarantee that the wall normal is always along the x_1 direction. Due to the periodic boundary conditions, two DWs exist in the system, and the system size is chosen to be sufficiently large to avoid the interactions between the two walls.

The DW energies of the nine possible types of walls obtained from the phase-field simulations are given in Table II, and the first-principles calculation results are included for comparison.[15] The agreement from our phenomenological predictions and the first-principles are quite reasonable, considering the fact that there are numerical and systematic errors in both methods.

As predicted by the rotational compatibility condition, the $[\bar{1}11,\bar{1}11](100)[\bar{1}\bar{1}\bar{1},111]$ (109°) DW has the lowest energy in Table II and the $[111,111](100)[111,\bar{1}\bar{1}\bar{1}]$ (OT) DW has a lower energy than the other two pure OT DWs. It is interesting to note that the two DWs were also predicted by Beanland.[11] The DWs with the second and third lowest energies are $[111,111](1\bar{1}0)[\bar{1}\bar{1}\bar{1},111]$ (180°) and $[\bar{1}\bar{1}1,\bar{1}\bar{1}1](1\bar{1}0)[\bar{1}\bar{1}\bar{1},\bar{1}\bar{1}\bar{1}]$ (71°), respectively. The three DWs with the lowest energies were extensively studied using first-principles calculations[15, 20-22] (the calculated DW energies from different groups are listed in Table SII).

To understand the origins of the relative magnitudes of the three lowest energies, we plot the order parameter profiles across the three DWs obtained from the phase-field simulations in Fig. 3 (c), (d) and (e). They are qualitatively consistent with the first-principles calculations and experimental measurements.[21] It should be noted that the first-principles calculations were performed at 0K, and the DW width is smaller than our values obtained at room temperature. As shown in Fig. 3 (c), the $[\bar{1}11,\bar{1}11](100)[\bar{1}\bar{1}\bar{1},111]$ (109°) DW satisfies the rotational compatibility condition (also listed in Table I). The OT pattern at the DW is $a^-a^-c^+$, similar to that in *Pnma*, the space group of the high temperature BFO.[14] This DW structure was also observed in Ref. [15], and is believed to be related to the high conductivity at the DW.[6] The $[\bar{1}\bar{1}1,\bar{1}\bar{1}1](1\bar{1}0)[\bar{1}\bar{1}\bar{1},\bar{1}\bar{1}\bar{1}]$ (71°) DW (Fig. 3e), however, does not satisfy the rotational compatibility condition since the wall normal

is not along any pseudocubic axes. Therefore, the energy and width of the 71° DW are much larger than those of the 109° DW. Furthermore, as shown in Fig. 3(d), [111,111](1$\bar{1}$0)[$\bar{1}\bar{1}\bar{1}$,111] (180°) is a pure FE DW without notable variations of the OT order parameters. Due to the relative contribution of variations of the polarization and OTs in the total free energy, the width and energy of the 180° DW are between those of the 71° and 109° DWs.

The analysis of the DW energies and order parameter profiles in BFO demonstrates the substantial contribution of the OTs to the DW energy anisotropy and DW thickness. Apparently, if the DW energies were dominated by the polarization gradient energy, the sequence of relative DW energies should be 71° <109° <180°, as in the rhombohedral $BaTiO_3$.[23, 24] Comparing the energies of the nine DWs in Table II, we found that if the OTs are parallel to the polarization, the sequence 71° <109° <180° is valid. However, as shown in Fig. 3 (b), due to the unit cell doubling, it is possible that the OTs are antiparallel to the polarization, which gives smaller DW energies in [$\bar{1}$11,$\bar{1}$11](100)[$\bar{1}\bar{1}\bar{1}$,111] (109°) and [111,111](1$\bar{1}$0)[$\bar{1}\bar{1}\bar{1}$,111] (180°). The DW energy sequence in BFO is thus changed to 109° <180° <71°. Earlier experiments in BFO thin films also support this unusual sequence, which showed that both the 109° and 180° DWs have lower DW energies than the 71° DWs.[25-28] Therefore, it is not sufficient to consider the polarization gradient alone to obtain the DW energy and its anisotropy in BFO.

To conclude, the specific corner-connecting feature of the oxygen octahedral network is shown to be responsible for the strong anisotropy of the domain wall (DW) energy in perovskites with oxygen octahedral tilt (OT) instability. It is demonstrated that there exist universal low-energy DWs, the orientations of which can be determined by the proposed rotational compatibility condition. This anisotropy can be described by the relation, $\kappa_{11} << \kappa_{44}$, in the gradient energy coefficient tensor within the framework of the Ginzburg-Landau-Devonshire

theory. The proposed new condition can serve as guidance to DW engineering in perovskites, and predict the low-energy OT DWs and consequently polarization DWs in the hybrid improper ferroelectrics, such as some Ruddlesden-Popper phases.[3, 29]

Acknowledgments: We are grateful to B. VanLeeuwen for discussions of Beanland's description. This work is supported by the NSF MRSEC under Grant No. DMR-0820404 and DMR-1210588 (FX and YJ). YW's effort is supported by the U.S. Department of Energy, Office of Basic Energy Sciences, Division of Materials Sciences and Engineering under Award No. DEFG02-07ER46417. The computer simulations were carried out on the LION and cyberstar clusters at the Pennsylvania State University, in part supported by instrumentation (cyberstar Linux cluster) funded by the NSF through Grant OCI-0821527.

References

[1] D. G. Schlom, L. Q. Chen, X. Pan, A. Schmehl, and M. A. Zurbuchen, Journal of the American Ceramic Society **91**, 2429 (2008).

[2] M. E. Lines and A. M. Glass, *Principles and Applications of Ferroelectrics and Related Materials* (Oxford University Press, Oxford, 1977).

[3] J. M. Rondinelli and C. J. Fennie, Advanced Materials **24**, 1961 (2012).

[4] W. Zhong and D. Vanderbilt, Physical Review Letters **74**, 2587 (1995).

[5] P. J. Ryan, et al., Nature Communications **4**, 1334 (2013).

[6] G. Catalan, J. Seidel, R. Ramesh, and J. F. Scott, Reviews of Modern Physics **84**, 119 (2012).

[7] J. Fousek and V. Janovec, Journal of Applied Physics **40**, 135 (1969).

[8] A. Glazer, Acta Crystallographica Section B: Structural Crystallography and Crystal Chemistry **28**, 3384 (1972).

[9] A. K. Tagantsev, E. Courtens, and L. Arzel, Physical Review B **64**, 224107 (2001).

[10] A. K. Tagantsev, L. E. Cross, and J. Fousek, *Domains in ferroic crystals and thin films* (Springer, 2010).

[11] R. Beanland, Acta Crystallographica Section A: Foundations of Crystallography **67**, 191 (2011).

[12] W. Cao and G. R. Barsch, Physical Review B **41**, 4334 (1990).

[13] W. G. Stirling, Journal of Physics C: Solid State Physics **5**, 2711 (1972).

[14] G. Catalan and J. F. Scott, Advanced Materials **21**, 2463 (2009).

[15] O. Dieguez, P. Aguado-Puente, J. Junquera, and J. Iniguez, Physical Review B **87**, 024102 (2013).

[16] P. Marton, I. Rychetsky, and J. Hlinka, Physical Review B **81**, 144125 (2010).

[17] W. L. Zhong, Y. G. Wang, P. L. Zhang, and B. D. Qu, Physical Review B **50**, 698 (1994).

[18] N. A. Pertsev, A. G. Zembilgotov, and A. K. Tagantsev, Physical Review Letters **80**, 1988 (1998).

[19] L. Chen and J. Shen, Computer Physics Communications **108**, 147 (1998).

[20] A. Lubk, S. Gemming, and N. Spaldin, Physical Review B **80**, 104110 (2009).

[21] Y. Wang, C. Nelson, A. Melville, B. Winchester, S. Shang, Z.-K. Liu, D. G. Schlom, X. Pan, and L.-Q. Chen, Physical Review Letters **110**, 267601 (2013).

[22] W. Ren, Y. Yang, O. Diéguez, J. Íñiguez, N. Choudhury, and L. Bellaiche, Physical Review Letters **110**, 187601 (2013).

[23] E. A. Eliseev, P. V. Yudin, S. V. Kalinin, N. Setter, A. K. Tagantsev, and A. N. Morozovska, Physical Review B **87**, 054111 (2013).

[24] M. Taherinejad, D. Vanderbilt, P. Marton, V. Stepkova, and J. Hlinka, Physical Review B **86**, 155138 (2012).

[25] C. W. Huang, L. Chen, J. Wang, Q. He, S. Y. Yang, Y. H. Chu, and R. Ramesh, Physical Review B **80**, 140101 (2009).

[26] C. T. Nelson, et al., Nano Letters **11**, 828 (2011).

[27] F. Zavaliche, P. Shafer, R. Ramesh, M. Cruz, R. Das, D. Kim, and C. Eom, Applied physics letters **87**, 252902 (2005).

[28] S. Baek, et al., Nature materials **9**, 309 (2010).

[29] N. A. Benedek and C. J. Fennie, Physical Review Letters **106**, 107204 (2011).

[30] P. Radaelli, M. Marezio, H. Hwang, and S.-W. Cheong, Journal of Solid State Chemistry **122**, 444 (1996).

TABLE I. Fully rotation-compatible DWs in some popular perovskites. In the notation $[\theta_i\theta_j\theta_k](n_in_jn_k)[\theta'_i\theta'_j\theta'_k]$, $[\theta_i\theta_j\theta_k]$ and $[\theta'_i\theta'_j\theta'_k]$ are the OT order parameters describing the OT patters in the two neighboring domains across a DW, and $(n_in_jn_k)$ is the DW normal. An asteroid superscript indicates an in-phase tilt (otherwise, out-of-phase tilt)

Space group of bulk phase (Glazer notation)	**Low-energy DW (local Glazer notation)**	**Examples[8, 30]**
$P4/mbm(a^0a^0c^+)$	$[001^*](001)[00\bar{1}^*](a^0a^0c^-)$	$NaNbO_3$
$I4/mcm(a^0a^0c^-)$	$[001](001)[00\bar{1}](a^0a^0c^+)$	$SrTiO_3$
$I4/mmm(a^0b^+b^+)$	$[01^*1^*](010)[0\bar{1}^*1^*](a^ob^-c^+)$	——
$Im ma(a^0b^-b^-)$	$[011](010)[0\bar{1}1](a^ob^+c^-)$	$La_{0.7}Ba_{0.3}MnO_3$
$Im\bar{3}(a^+a^+a^+)$	$[1^*1^*1^*](100)[\bar{1}^*1^*1^*](a^-b^+b^+)$	$Ca_{0.25}Cu_{0.75}MnO_3$
$R3c(a^-a^-a^-)$	$[111](100)[\bar{1}11](a^+b^-b^-)$	$BiFeO_3$, $PbZrO_3$
$Pnma(a^-a^-c^+)$	$[11^*1^*](001)[11\bar{1}^*](a^-a^-c^-)$ $[11^*1^*](100)[\bar{1}11^*](a^+b^-c^+)$	$CaTiO_3$, $GdFeO_3$

TABLE II. DW Energies (mJ/m^2) of the nine types of DWs in BFO. The angles after the DW notation measure the changes of the polarization vectors in the neighboring domains across a DW.

DW type	**Dieguez *et al.*[15]**	**From our work**
$[111,111](100)[111,\bar{1}\bar{1}\bar{1}]$ (OT)	227	231
$[111,111](110)[111,\bar{1}\bar{1}\bar{1}]$ (OT)	254	293
$[1\bar{1}1,1\bar{1}1](110)[1\bar{1}1,\bar{1}\bar{1}\bar{1}]$ (OT)	293	290
$[\bar{1}\bar{1}1,\bar{1}\bar{1}1](1\bar{1}0)[\bar{1}\bar{1}\bar{1},\bar{1}\bar{1}\bar{1}]$ (71°)	152	124
$[\bar{1}\bar{1}1,\bar{1}\bar{1}1](1\bar{1}0)[\bar{1}\bar{1}\bar{1},111]$ (71°)	178	161
$[\bar{1}11,\bar{1}11](100)[\bar{1}\bar{1}\bar{1},111]$ (109°)	62	55
$[\bar{1}11,\bar{1}11](100)[\bar{1}\bar{1}\bar{1},\bar{1}\bar{1}\bar{1}]$ (109°)	319	259
$[111,111](1\bar{1}0)[\bar{1}\bar{1}\bar{1},111]$ (180°)	74	94
$[111,111](1\bar{1}0)[\bar{1}\bar{1}\bar{1},\bar{1}\bar{1}\bar{1}]$ (180°)	255	381

Figure Legends

FIG. 1. Green and blue diamonds represent oxygen octahedra rotated clockwise and counterclockwise, respectively, with the rotation axis along x_3. The balls inside the diamonds represent B atoms. Red and orange balls refer to oxygen and A atoms, respectively. (a) and (b) show the OT patterns in $a^0a^0c^-$ and $a^0a^0c^+$ phases. (c) and (d) demonstrate type-I walls in $a^0a^0c^-$ and $a^0a^0c^+$ phases. The dot-dashed lines indicate the locations of DWs. Schematic plot of oxygen atom displacements in (e) type-I wall in $a^0a^0c^-$, (f) type-I wall in $a^0a^0c^+$, (g) type-II wall in $a^0a^0c^-$, and (h) type-I wall in $a^0b^-b^-$. Circles indicate oxygen atoms. Every shared oxygen atom at the DWs is artificially split into two virtual atoms (dotted circles) in (e), (f), (g), and (h), in order to more clearly show the displacements of the oxygen atoms in each domain. A cross or a dot in a circle represents an atom displacement of into-plane or out-of-plane, respectively.

FIG. 2. (a) Magnitude of κ_{eff} along the direction (ω,η) with x_3 as the polar axis. The OT rotates around the x_3 axis. (b) Magnitude of κ_{eff} in the x_1x_3 plane. Also shown are the magnitudes of κ'_{11} and κ'_{44}, the gradient coefficients in the rotated coordinate system.

FIG. 3. (a) and (b) 1D schematic plot of an (a) FE+OT DW (left: $P_3=1,\theta_3=1$, right: $P_3=-1,\theta_3=-1$), and (b) pure FE DW (left: $P_3=1,\theta_3=1$, right: $P_3=-1,\theta_3=1$). OTs are represented by diamonds of different colors; a dot and a cross in a circle indicate polarization pointing out-of-plane and into-plane, respectively. Plotted in (c), (d) and (e) are order parameter profiles of (c) $[\bar{1}1\bar{1},\bar{1}11](100)[\bar{1}\bar{1}\bar{1},111]$ (109°), (d) $[111,111](1\bar{1}0)[\bar{1}\bar{1}\bar{1},111]$ (180°) and (e) $[\bar{1}\bar{1}1,\bar{1}\bar{1}1](1\bar{1}0)[\bar{1}\bar{1}\bar{1},\bar{1}\bar{1}\bar{1}]$ (71°) DWs.

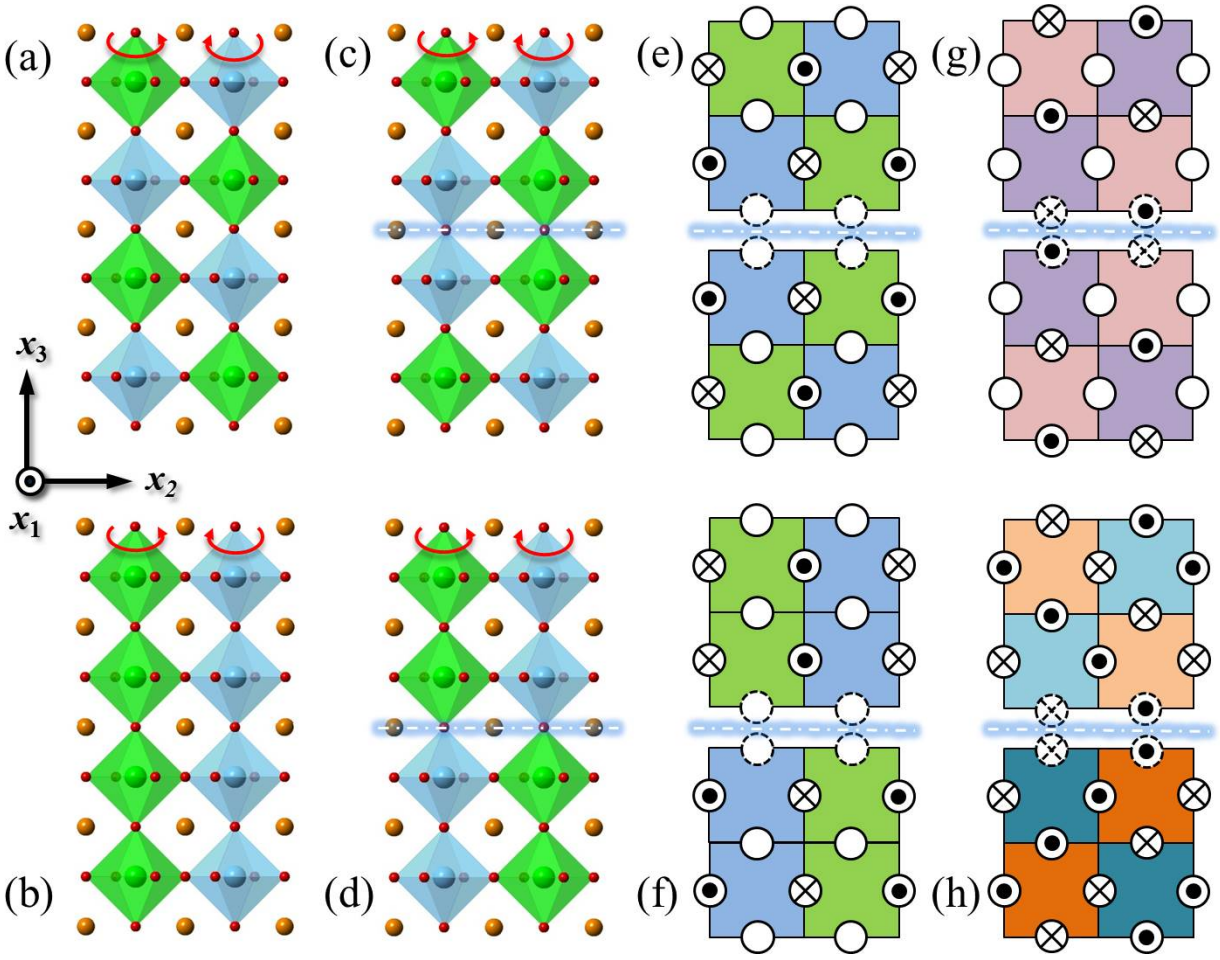

Figure 1

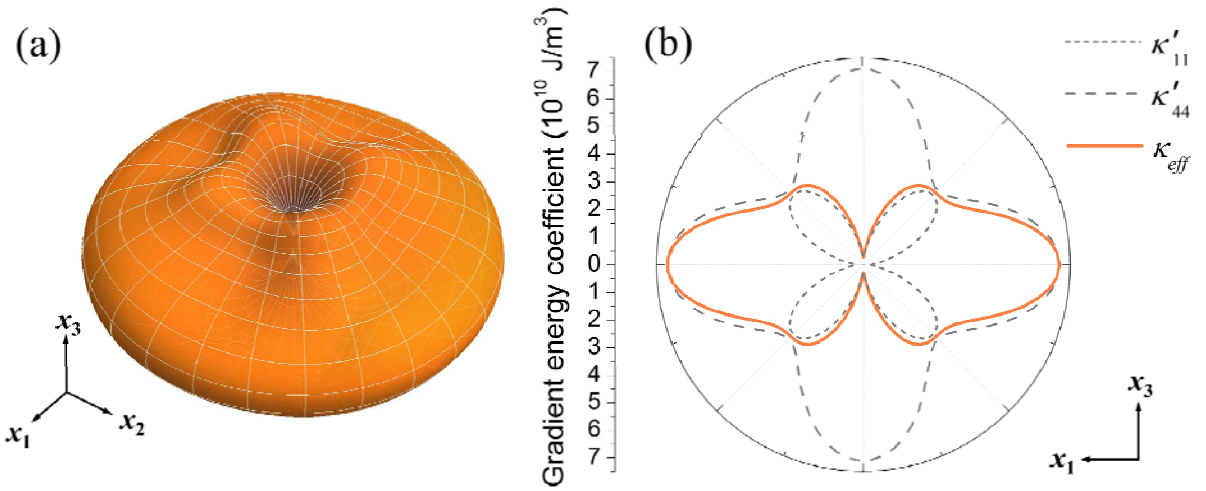
(a)
x_3
x_1
x_2
Gradient energy coefficient (10^{10} J/m^3)
7
6
5
4
3
2
1
0
1
2
3
4
5
6
7
(b)
κ'_{11}
κ'_{44}
κ_{eff}
x_3
x_1

Figure 2

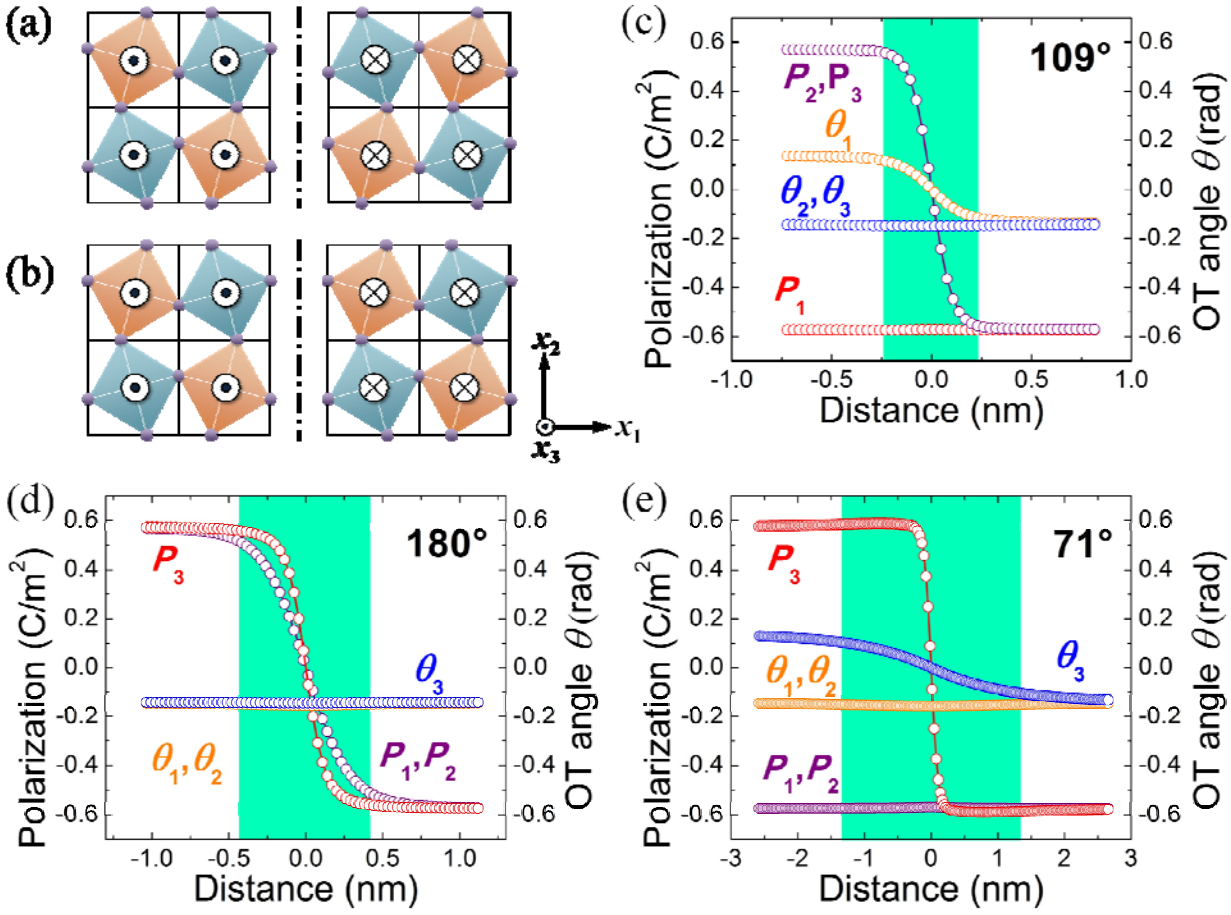
(a)
(b)
x_2
x_1
x_3
(c)
109°
P_2,P_3
θ_1
θ_2,θ_3
P_1
Polarization (C/m^2)
OT angle θ(rad)
Distance (nm)
(d)
180°
P_3
θ_3
θ_1,θ_2
P_1,P_2
(e)
71°
P_3
θ_1,θ_2
θ_3
P_1,P_2

Figure 3